




High resolution femtosecond direct laser writing with wrapped lens

ANDREA TOULOUSE,^{1,2,*}  SIMON THIELE,^{1,2,3} KAI HIRZEL,^{4,5}
MICHAEL SCHMID,^{2,6} KSENIA WEBER,^{2,6}  MARIA ZYRIANOVA,^{4,7}
HARALD GIESSEN,^{2,6}  ALOIS M. HERKOMMER,^{1,2} AND MICHAEL
HEYMANN^{4,5,8}

¹*Institute of Applied Optics (ITO), University of Stuttgart, Pfaffenwaldring 9, 70569 Stuttgart, Germany*

²*Stuttgart Research Center of Photonic Engineering (SCoPE), University of Stuttgart, Pfaffenwaldring 57, 70569 Stuttgart, Germany*

³*Printoptix GmbH, Johannesstraße 11, 70176 Stuttgart, Germany*

⁴*Institute of Biomaterials and Biomolecular Systems (IBBS), University of Stuttgart, Pfaffenwaldring 57, 70569 Stuttgart, Germany*

⁵*Stuttgart Research Center Systems Biology (SRCBS), University of Stuttgart, Nobelstr. 15, 70569 Stuttgart, Germany*

⁶*4th Physics Institute (PI4), University of Stuttgart, Pfaffenwaldring 57, 70569 Stuttgart, Germany*

⁷*Institute of Interfacial Process Engineering and Plasma Technology (IGVP), University of Stuttgart, Nobelstr. 12, 70569 Stuttgart, Germany*

⁸*michael.heyman@bio.uni-stuttgart.de*

**andrea.toulouse@ito.uni-stuttgart.de*

Abstract: Wrapped writing mode is a simple, inexpensive approach to multiphoton stereolithography. Standard $\sim 10\ \mu\text{m}$ thin cling foil shields the objective from direct contact with the photoresist, without compromising writing resolution. A diffraction limited lateral voxel width below 150 nm was demonstrated through ray tracing simulations and electron microscopy using standard polymer photoresist. Wrapped mode, like dip-in printing, is not limited by the objective working distance height. Its utility to prototype new print resists was validated through custom aqueous protein, silver nitrate, and black epoxy based formulations.

© 2022 Optica Publishing Group under the terms of the [Optica Open Access Publishing Agreement](#)

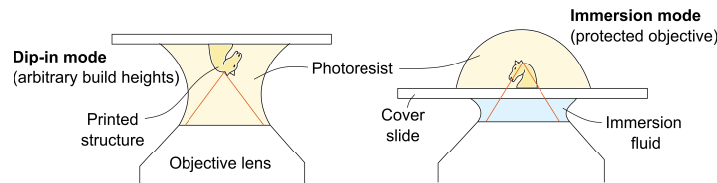
1. Introduction

Multiphoton polymerization was pioneered in the 1990s to fabricate 3D nano- and microstructures [1–3] and continued to evolve into several femtosecond direct laser writing (fs DLW) methods since then [4–10]. Their applications include simple waveguide coupling elements [11], complex micro-optical systems [12–16], microfluidics [17], cell [18,19] and synthetic biology [20,21], metamaterial engineering [22], and metallic microelectronics [23], to name a few.

Ideal fs DLW modes are unlimited in attainable fabrication height and minimize optical aberrations, while avoiding direct contact between photoresist and the objective (Fig. 1). In dip-in mode, the photoresist itself serves as immersion medium to allow for arbitrary build heights [8,24]. Disadvantages are the need for suitable index matching of the resist, as well as the delicate and often time-consuming cleaning of the objective to not risk degrading the objective's sealings or coatings. This constrains permissive solvents in engineering novel photoresists, especially when nanocomposite, protein, or metal-deposition chemistry are used [19,25–29]. Alternatively, the laser is focused in immersion through a glass substrate into the photoresist (immersion mode). Here, new resist formulations can be tested by a simple swap of the substrate, but feasible fabrication heights are limited to below the working distance of the objective, and aberrations from polymerized resist reduce print quality. The growing demand for application-tailored photoresist formulations would hence benefit from an immersed printing mode that is no longer

restricted in fabrication height. This was first achieved by locating the photoresist in a material vat held at a steady immersion, while the printing substrate is moved out of the vat during fabrication [30]. Vat mode printing, however, may be difficult to implement on existing hardware. Also, writing objectives are typically not designed for use in a threefold material system of immersion, cover glass, and photoresist which limits the accessible print resolution. All these considerations motivated us to seek an alternative solution.

A Conventional fs DLW modes



B Wrapped fs DLW mode

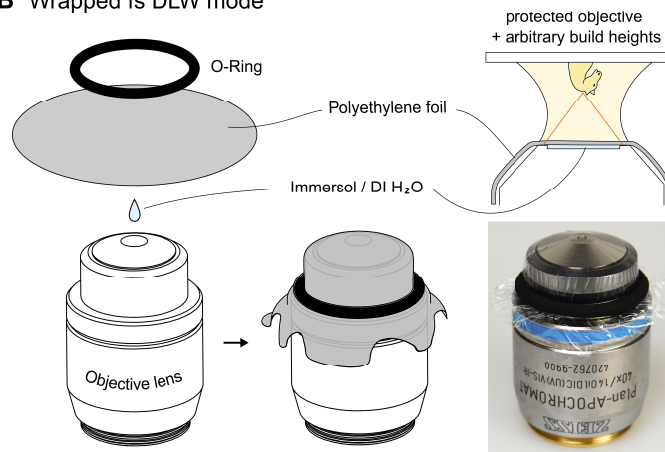


Fig. 1. Femtosecond direct laser writing modes. **(A)** The writing objective is in direct contact with the photoresist in dip-in mode (left). While enabling large build heights, this configuration exposes the objective to the resist. In immersion mode (right), the objective is protected from contacting the photoresist directly by a cover glass and an immersion medium. However, feasible fabrication heights are limited to below the working distance of the objective. **(B)** Wrapped mode achieves large build heights without exposing the objective to the resist. A droplet of a standard immersion medium (oil or deionized water), a suitable foil, and an O-ring are assembled around the objective. The advantages of dip-in and immersion mode are thus combined in an inexpensive and easy-to-use approach.

Here, we present a wrapped fs DLW mode (Fig. 1(B)), where the objective is covered by a thin foil and secured in position with a suitable O-ring. This configuration keeps beam paths inside the immersion fluid and the protective foil very short in order to conserve printing resolution. It is simple to retrofit on any system by placing standard polyethylene (PE) kitchen cling foil, or more chemically resistant foils even with poorly matched refractive indices, onto the objective. As a result, any unconventional photoresist can be used in combination with arbitrary fs DLW writing objectives to achieve immersion-mode printing without limiting the fabrication heights by the objective working distance. For matched refractive indices of objective and photoresist, the print resolution is not compromised for a wide range of foil and immersion fluid refractive indices.

PE, or if needed pre-sterilized or more solvent resistant foils, can thus facilitate fs DLW of resists that require sterility or harsh solvents. Used objectives are easy to clean as the foil can be

directly disposed after printing. Conditions for diffraction limited wrapped mode resolution were assessed in optical simulations and experimentally confirmed. Finally, three custom photoresists were tested.

2. Simulations of wrapped writing mode performance envelope

Optical propagation (Fig. 2) was simulated in *Zemax OpticStudio*. The wavefront exiting from the writing objective was assumed to be perfectly spherical coming from a propagation medium matched to the refractive index of the photoresist (liquid IP-Dip, $n = 1.512$ at $\lambda = 780$ nm, $T = 20^\circ\text{C}$ [31]). In accordance with our experiments and standard fs DLW configurations, especially Numerical Apertures (NAs) of 1.4 and 0.8 were assessed. The propagation was simulated at 780 nm, the laser wavelength of the 3D-printers used in our experiments (Photonic Professional GT & GT2, Nanoscribe GmbH & Co. KG). Next, we accounted for the gap between foil and writing objective as defined by the protruding objective mount edge and front lens. Confocal microscopy quantified this gap height to be 0-40 μm for our objectives (Table 1, experimental section). Immersion media for this gap were set to immersion oil (Zeiss Immersol 518 F, $n = 1.509$ at $\lambda = 780$ nm) or deionized water ($n = 1.329$ at $\lambda = 780$ nm, $T = 20^\circ\text{C}$). The subsequent PE foil ($n = 1.544$ at $\lambda = 780$ nm, obtained from [32]) was modeled as a 10 μm

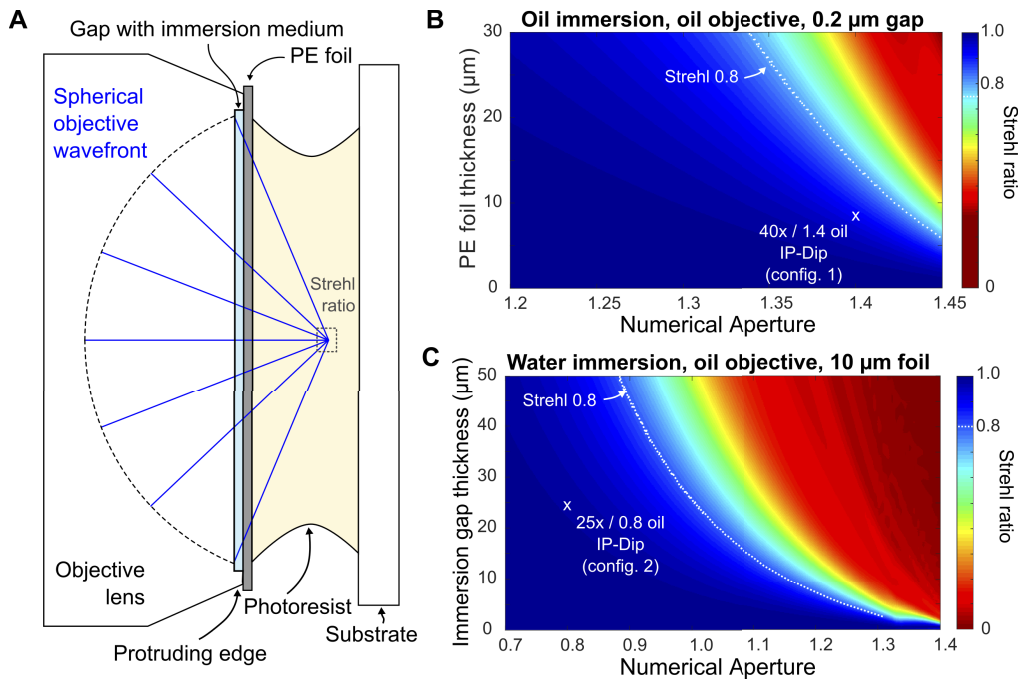


Fig. 2. Simulations of the diffraction limit in wrapped writing mode. (A) Simulation configuration: The objective wavefront was assumed to be perfectly spherical. Immersion gap and PE foil were defined as plane parallel plates and the Strehl ratio was analyzed in the focal point. (B) Strehl ratios simulated for oil immersion and different PE foil thicknesses at a fixed immersion gap thickness of 0.2 μm . A white dotted line delineates diffraction limited performance before writing resolution degrades at higher NA and foil thickness. (C) Strehl ratios for deionized water immersion and different gap thicknesses at a fixed PE foil thickness of 10 μm . Experimentally realized configs. 1 (40x) and 2 (25x) project diffraction limited performance.

thin plate in accordance with confocal microscopy measurements. These parameters reflect the standard configuration also used in our experiments. Sensitivity analyses use this configuration as starting point. Once transmitted through the PE foil, simulated rays enter the photoresist and culminate in the focal spot. The Strehl ratio was evaluated from the Huygens point spread function (PSF) at the best focus position in z which was refocused per data point. Strehl ratios of 0.8 and higher were considered as diffraction limited performance.

Table 1. Experimental print configurations in wrapped fs DLW mode. Writing objectives indicate the index media adjustment ring settings. Gap values denote measured heights between front lens and the protruding edge of the objective mount for the used objectives. Gap errors are experimental standard deviations.

config.	writing objective	NA	immersion	gap
1	40x oil	1.4	Immersol 518 F	$0.19 \pm 0.05 \mu\text{m}$
2	25x oil	0.8	DI H ₂ O	$24.4 \pm 0.4 \mu\text{m}$
3	25x water	0.8	DI H ₂ O	$24.4 \pm 0.4 \mu\text{m}$
4	25x oil	0.8	Immersol 518 F	$24.4 \pm 0.4 \mu\text{m}$
5	40x water	1.2	DI H ₂ O	$36.5 \pm 1.2 \mu\text{m}$

Simulations explored various objectives, immersion media, foil, and photoresist configurations for wrapped mode. First, the sensitivity to foil and gap thickness variations for different NAs was analyzed for both objectives (Fig. 2(B), (C)). The high resolution NA 1.4 setup (config. 1) with almost perfectly matched media achieved a diffraction limited Strehl ratio of 0.897 (Fig. 2(B)). Thicker PE foils and higher objective NA had markedly degraded resolution. The poorly matched low resolution NA 0.8 oil objective (config. 2) with water immersion in turn had a diffraction limited Strehl ratio of 0.981 (Fig. 2(C)). A wide range of NAs and water gap thicknesses achieved diffraction limited performance against a 10 μm PE foil.

The sensitivity to refractive index mismatches was compared between high NA 1.4 and low NA 0.8 objectives, with a 25 μm immersion gap and a 10 μm PE foil each (Fig. 3). Clearly, matching the objective wavefront to the photoresist is most critical and should not exceed $\Delta n = 0.005$ for NA 1.4. Thus, similar to dip-in mode, photoresist and objective should be carefully matched for high NAs. Accordingly, our approach of protecting the objective is not designed to overcome this restriction and we refer to the use of objective lenses with immersion adjustment rings here. Optical performance, however, is very insensitive to index mismatches of foil and immersion medium and especially uncritical for the low NA 0.8 setup. Even at high NA 1.4, diffraction limited printing was maintained across a wide range of index mismatches due to the short beam paths which allows our approach to utilize almost arbitrary immersion fluids and foil material combinations.

Overall, we conclude from the simulations that thinner immersion gaps and foils achieved best performance, or in other words shorter beam paths are less sensitive to higher refractive index mismatches. Higher numerical apertures in turn require better index matching for experimentally convenient gap and foil thicknesses.

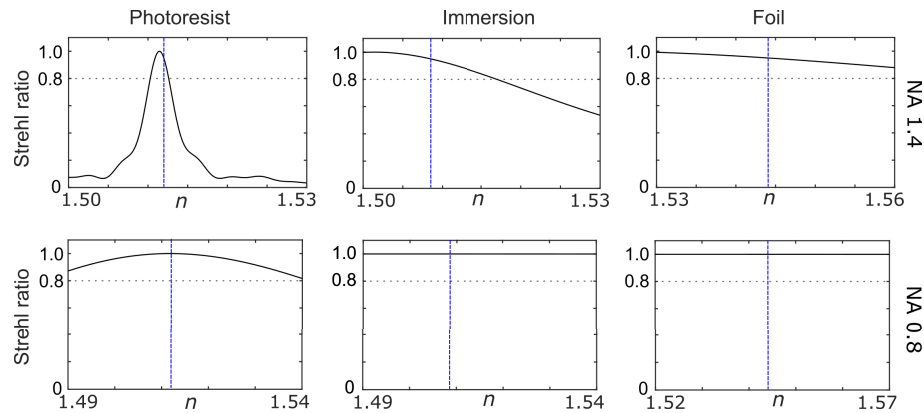


Fig. 3. Sensitivity to refractive index mismatches for an objective lens matched to $n = 1.512$ immersion (simulations). Strehl ratios were evaluated for exemplary high NA 1.4 and low NA 0.8 objectives for a 25 μm immersion gap and a 10 μm PE foil. Refractive indices were varied one at a time for the photoresist, the immersion medium, and the foil, respectively. For each variation, all other refractive indices were set to their standard configuration values given in the text and indicated with blue dashed lines in the graphs.

3. Experimental wrapped writing mode validation

Objectives were wrapped with low-cost kitchen cling foil (e.g. ALIO Frischhaltefolie, Wentus Kunststoff GmbH) (Fig. 4(A)). First, the immersion medium was applied to the objective's front lens. Second, the foil was stretched onto a simple 3D-printed fixture (material: polylactide (PLA) filament, fused filament printer: Ultimaker 3, Ultimaker B.V.). Third, the stretched foil was lowered over the objective, until it covered the front lens mount tightly to form an air bubble free thin immersion film between both. This procedure also disposed excess immersion medium to the sides. The assembly was secured with an O-ring of suitable diameter, rolled over the objective before the foil was cut and the clamping fixture removed. Finally, the standard or experimental photoresist was applied to the wrapped objective, shielded from the objective's front lens by the thin foil. Detailed experimental configurations are given in Tables 1 and 2.

Table 2. Overview of printed structures with wrapped fs DLW mode. Respective objective and immersion configurations are listed in Table 1.

config.	photoresist	printed structure
1	IP-Dip	woodpile ($\Delta x, \Delta y = 500 \text{ nm}$ / $\Delta z = 990 \text{ nm}$)
2	IP-Dip	woodpile ($\Delta x, \Delta y = 1 \mu\text{m}$ / $\Delta z = 2.12 \mu\text{m}$)
3	GM10 methacrylated gelatin [19,33]	mouse alveolar scaffold [19]
4	IP-Black prototype	rook (580 μm high)
5	silver nitrate [34]	wire grid (200 μm wide)

Experimentally achieved lateral ($\Delta x, \Delta y$) and axial (Δz) resolutions were identical when comparing wrapped mode with conventional dip-in mode across the objective field of view, as confirmed by comparing different writing field positions (Fig. 4). Woodpile scaffolds were printed from IP-Dip onto indium tin oxide coated substrates (both Nanoscribe GmbH & Co. KG), developed in propylene glycol methyl ether acetate, rinsed with isopropanol, and dried under nitrogen. After printing, the O-ring was removed from the objective to dispose the foil with excess resist. Residual immersion oil was cleaned or reused. Thin DI H_2O immersion films quickly dried off without residuals. Resulting voxel dimensions were examined by scanning electron

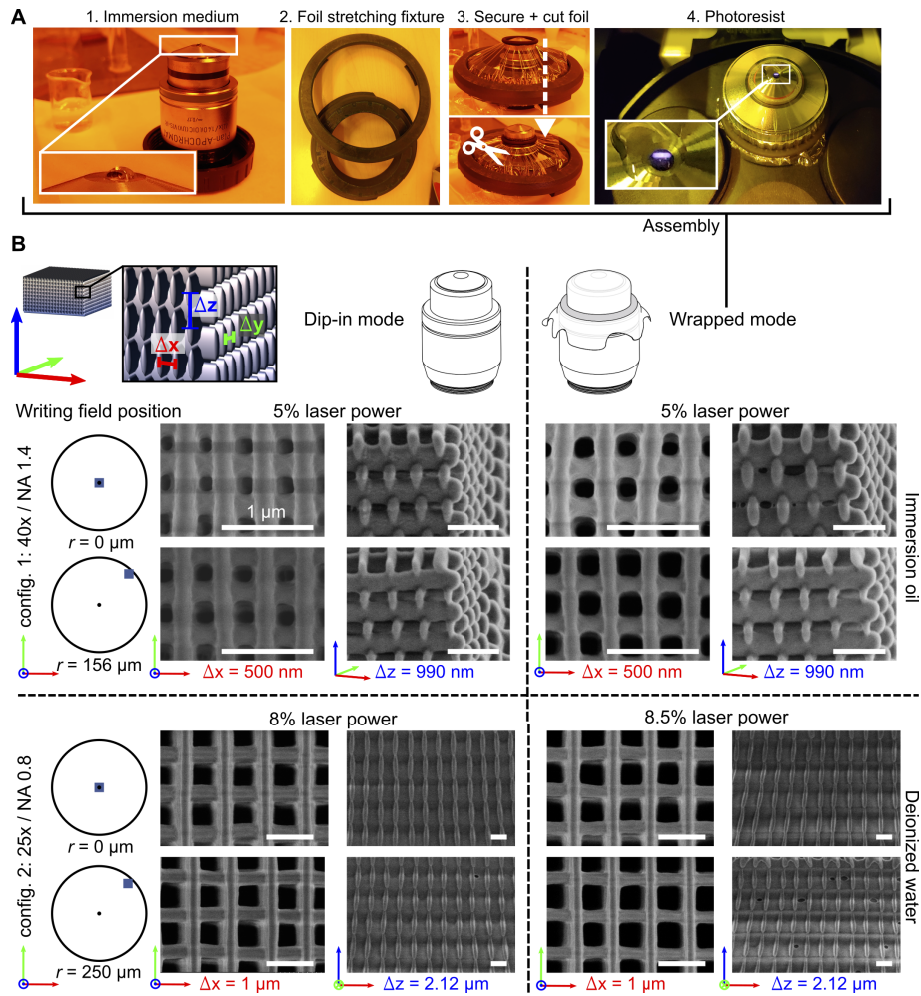


Fig. 4. Experimental wrapped mode assembly and resolution limit. **(A)** Immersion medium is placed onto the objective. A stretching fixture helps to place the foil and to secure it with an O-ring. After trimming the foil, the objective is ready for fs DLW. **(B)** Dip-in mode (left) and wrapped mode (right) resolution was assessed from fabricated woodpile structures via scanning electron microscopy, both in the writing field center ($r = 0$) and off axis ($r = 156 \mu\text{m}$ and $r = 250 \mu\text{m}$) for oil immersion and water immersion with the 40x oil and 25x oil objective, respectively. See Table 1 and 2 for configuration details.

microscopy. The 40 \times oil, 1.4 NA high resolution achieved config. 1 lateral voxel diameters below 150 nm, suggesting diffraction limited performance in accordance with our simulations. Marginally thinner voxel lines for wrapped mode in the off-center writing field position indicate a slightly higher polymerization threshold in the field. Most importantly, however, achievable print resolution was maintained. The low resolution 25x oil, 0.8 NA objective water immersion config. 2 also achieved voxel dimensions similar to conventional dip-in writing, albeit at marginally higher laser powers. This polymerization threshold increase from the 8% dip-in control to 8.5% suggests an increase of the focal spot size, which however can be easily compensated through laser power adjustments. Both, simulated and experimental data confirm that our inexpensive approach to protect the microscope objective from contact with the photoresist can be readily

implemented on existing fs DLW hardware with almost no performance loss across the full writing field of view.

To evaluate the utility of wrapped mode for developing new photoresists, we chose three alternative resist chemistries (Fig. 5). First, fs DLW bio-ink engineering was explored. Protein-based photoresist containing 25 wt% GM10, a gelatin derivative with a high degree of methacrylation, and 2 wt% LAP (lithium phenyl-2,4,6-trimethylbenzoylphosphinate) photo-initiator was prepared in phosphate buffer to print a geometry derived from *in vivo* mouse lung parenchymal tissue containing entire alveoli, as previously described [19]. Resulting cell scaffolds fabricated in water immersion wrapped mode (25x water, NA 0.8 objective) were not distinguishable from dip-in control prints. The ease of replacing the wrapped mode foil reduces biological contamination risks and favors maintained sterile working conditions. Second, a 580 μm high rook was fabricated from highly absorptive IP-Black photoresist. Hence, fabrication of structures extending well beyond the working distance of the writing objective was feasible (210 μm working distance at 170 μm cover glass thickness 25x oil, NA 0.8 objective). Direct exposure in conventional dip-in mode would risk irreversible black stains on the objective's front lens. Conventional immersion mode printing in turn would not allow printing such a 580 μm high structure. Furthermore, continuously changing absorptive beam paths in the black photoresist would be problematic for polymerization threshold conservation in immersion mode printing. As a third example, we fabricated a silver wire grid from a water-based silver precursor (silver nitrate AgNO_3 , ammonia NH_3 , and a trisodium citrate $\text{Na}_3\text{C}_6\text{H}_5\text{O}_7$ initiator [34]) in wrapped mode (40x water, NA 1.2 objective). Depositing a metal film onto an unprotected objective lens in conventional dip-in mode may cause irrevocable damage to the objective, a risk that is highly reduced in wrapped mode.

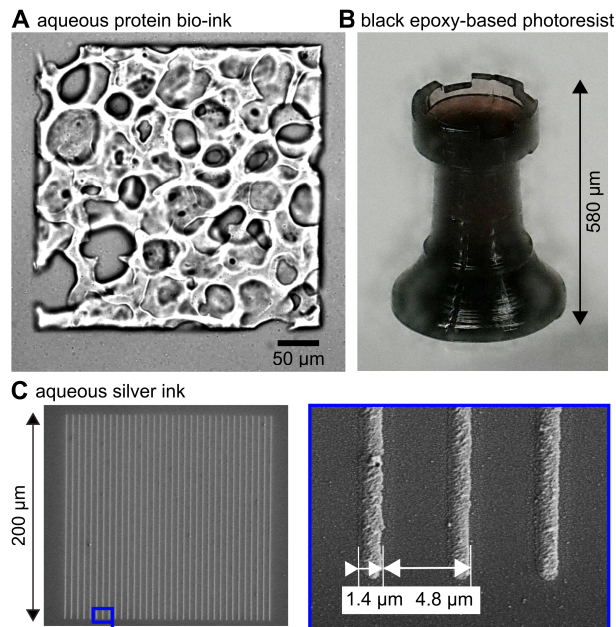


Fig. 5. Wrapped mode application examples with custom photoresists. (A) Brightfield micrograph during fabrication of a 3D cell scaffold from aqueous protein photoresist (config. 3). (B) Micrograph of a developed 580 μm high rook printed from IP-Black prototype resist (config. 4). (C) Electron microscopy of a metal wire grid printed from aqueous silver precursor (config. 5). Compare Table 1 and 2 for detailed print configurations.

4. Conclusion

In conclusion, wrapped writing mode combines the strengths of immersion and dip-in mode fs DLW printing: protecting the objective while maintaining a diffraction limited resolution without working distance limitations. It is simple and inexpensive to implement, has an extensive performance envelope, and is hence ideally suited to spur future photoresist development efforts.

Funding. Deutsche Forschungsgemeinschaft (GRK2642); Vector Stiftung (MINT Innovationen); Ministerium für Wissenschaft, Forschung und Kunst Baden-Württemberg (3R-Netzwerk BW, ICM, Leistungszentrum Mass Personalization, RiSC); European Research Council (3DPRINTEDOPTICS, 862549, COMPLEXPLAS); Baden-Württemberg Stiftung (OPTERIAL); Bundesministerium für Bildung und Forschung (13N10146, PRINTFUNCTION, PRINTOPTICS).

Acknowledgments. We thank Alexander Southan and Jana Grübel (IGVP, University of Stuttgart) for discussions and synthesizing GM10.

Disclosures. A patent application was filed (10985P0003DE).

Data availability. Data underlying the results presented in this paper are not publicly available at this time but may be obtained from the authors upon reasonable request.

References

1. J. H. Strickler and W. W. Webb, "Two-photon excitation in laser scanning fluorescence microscopy," in *Proc. SPIE 1398, CAN-AM Eastern '90*, (1991), pp. 107–118.
2. E.-S. Wu, J. H. Strickler, W. R. Harrell, and W. W. Webb, "Two-photon lithography for microelectronic application," in *Proc. SPIE 1674, Optical/Laser Microlithography V*, (1992), p. 776.
3. S. Maruo, O. Nakamura, and S. Kawata, "Three-dimensional microfabrication with two-photon-absorbed photopolymerization," *Opt. Lett.* **22**(2), 132 (1997).
4. H.-B. Sun and S. Kawata, "Two-photon photopolymerization and 3D lithographic microfabrication," in *NMR • 3D Analysis • Photopolymerization*, vol. 170 of *Advances in Polymer Science* (Springer Berlin Heidelberg, 2004), pp. 169–273.
5. C. Liberale, G. Cojoc, P. Candeloro, G. Das, F. Gentile, F. de Angelis, and E. Di Fabrizio, "Micro-optics fabrication on top of optical fibers using two-photon lithography," *IEEE Photonics Technol. Lett.* **22**(7), 474–476 (2010).
6. M. Thiel and M. Hermatschweiler, "Three-dimensional laser lithography," *Optik & Photonik* **6**(4), 36–39 (2011).
7. K. Sugioka and Y. Cheng, "Femtosecond laser three-dimensional micro- and nanofabrication," *Appl. Phys. Rev.* **1**(4), 041303 (2014).
8. J. K. Hohmann, M. Renner, E. H. Waller, and G. von Freymann, "Three-dimensional μ -printing: an enabling technology," *Adv. Opt. Mater.* **3**(11), 1488–1507 (2015).
9. M. Malinauskas, A. Žukauskas, S. Hasegawa, Y. Hayasaka, V. Mizeikis, R. Buividas, and S. Juodkazis, "Ultrafast laser processing of materials: from science to industry," *Light: Sci. Appl.* **5**(8), e16133 (2016).
10. G. Berglund, A. Wisniewiecki, J. Gawedzinski, B. Applegate, and T. S. Tkaczyk, "Additive manufacturing for the development of optical/photonics systems and components," *Optica* **9**(6), 623 (2022).
11. P.-I. Dietrich, M. Blaicher, I. Reuter, M. Billah, T. Hoose, A. Hofmann, C. Caer, R. Dangel, B. Offrein, U. Troppenz, M. Moehle, W. Freude, and C. Koos, "In situ 3D nanoprinting of free-form coupling elements for hybrid photonic integration," *Nat. Photonics* **12**(4), 241–247 (2018).
12. T. Gissibl, S. Thiele, A. Herkommer, and H. Giessen, "Two-photon direct laser writing of ultracompact multi-lens objectives," *Nat. Photonics* **10**(8), 554–560 (2016).
13. S. Thiele, K. Arzenbacher, T. Gissibl, H. Giessen, and A. M. Herkommer, "3D-printed eagle eye: compound microlens system for foveated imaging," *Sci. Adv.* **3**(2), e1602655 (2017).
14. S. Schmidt, S. Thiele, A. Toulouse, C. Bösel, T. Tiess, A. Herkommer, H. Gross, and H. Giessen, "Tailored micro-optical freeform holograms for integrated complex beam shaping," *Optica* **7**(10), 1279 (2020).
15. A. Toulouse, J. Drozella, S. Thiele, H. Giessen, and A. Herkommer, "3D-printed miniature spectrometer for the visible range with a $100 \times 100 \mu\text{m}^2$ footprint," *Light: Adv. Manuf.* **2**(1), 20–30 (2021).
16. A. Toulouse, J. Drozella, P. Motzfeld, N. Fahrback, V. Aslani, S. Thiele, H. Giessen, and A. M. Herkommer, "Ultra-compact 3D-printed wide-angle cameras realized by multi-aperture freeform optical design," *Opt. Express* **30**(2), 707 (2022).
17. J. Knoška, L. Adriano, S. Awel, K. R. Beyerlein, O. Yefanov, D. Oberthuer, G. E. Peña Murillo, N. Roth, I. Sarrou, P. Villanueva-Perez, M. O. Wiedorn, F. Wilde, S. Bajt, H. N. Chapman, and M. Heymann, "Ultracompact 3D microfluidics for time-resolved structural biology," *Nat. Commun.* **11**(1), 657 (2020).
18. C. Barner-Kowollik, M. Bastmeyer, E. Blasco, G. Delaitre, P. Müller, B. Richter, and M. Wegener, "3D laser micro- and nanoprinting: challenges for chemistry," *Angew. Chem. Int. Ed.* **56**(50), 15828–15845 (2017).
19. A. Erben, M. Hörning, B. Hartmann, T. Becke, S. A. Eisler, A. Southan, S. Cranz, O. Hayden, N. Kneidinger, M. Königshoff, M. Lindner, G. E. M. Tovar, G. Burgstaller, H. Clausen-Schaumann, S. Sudhop, and M. Heymann, "Precision 3D-printed cell scaffolds mimicking native tissue composition and mechanics," *Adv. Healthcare Mater.* **9**(24), 2000918 (2020).

20. Z.-C. Ma, Y.-L. Zhang, B. Han, X.-Y. Hu, C.-H. Li, Q.-D. Chen, and H.-B. Sun, "Femtosecond laser programmed artificial musculoskeletal systems," *Nat. Commun.* **11**(1), 4536 (2020).
21. H. Eto, H. G. Franquelim, M. Heymann, and P. Schwill, "Membrane-coated 3D architectures for bottom-up synthetic biology," *Soft Matter* **17**(22), 5456–5466 (2021).
22. T. Bückmann, M. Thiel, M. Kadic, R. Schittny, and M. Wegener, "An elasto-mechanical unfeelability cloak made of pentamode metamaterials," *Nat. Commun.* **5**(1), 4130 (2014).
23. Z.-C. Ma, Y.-L. Zhang, B. Han, Q.-D. Chen, and H.-B. Sun, "Femtosecond-laser direct writing of metallic micro/nanostructures: from fabrication strategies to future applications," *Small Methods* **2**(7), 1700413 (2018).
24. T. Bückmann, N. Stenger, M. Kadic, J. Kaschke, A. Frölich, T. Kennerknecht, C. Eberl, M. Thiel, and M. Wegener, "Tailored 3D mechanical metamaterials made by dip-in direct-laser-writing optical lithography," *Adv. Mater.* **24**(20), 2710–2714 (2012).
25. F. Kotz, A. S. Quick, P. Risch, T. Martin, T. Hoose, M. Thiel, D. Helmer, and B. E. Rapp, "Two-photon polymerization of nanocomposites for the fabrication of transparent fused silica glass microstructures," *Adv. Mater.* **33**(9), 2006341 (2021).
26. K. Weber, D. Werdehausen, P. König, S. Thiele, M. Schmid, M. Decker, P. W. de Oliveira, A. Herkommer, and H. Giessen, "Tailored nanocomposites for 3D printed micro-optics," *Opt. Mater. Express* **10**(10), 2345 (2020).
27. J. D. Pitts, P. J. Campagnola, G. A. Epling, and S. L. Goodman, "Submicron multiphoton free-form fabrication of proteins and polymers: Studies of reaction efficiencies and applications in sustained release," *Macromolecules* **33**(5), 1514–1523 (2000).
28. M. Farsari and B. N. Chichkov, "Materials processing: two-photon fabrication," *Nat. Photonics* **3**(8), 450–452 (2009).
29. M. Malinauskas, A. Žukauskas, K. Belazaras, K. Tikuišis, V. Purlys, R. Gadonas, and A. Piskarskas, "Laser fabrication of various polymer microoptical components," *Eur. Phys. J. Appl. Phys.* **58**(2), 20501 (2012).
30. K. Obata, A. El-Tamer, L. Koch, U. Hinze, and B. N. Chichkov, "High-aspect 3D two-photon polymerization structuring with widened objective working range (wow-2pp)," *Light: Sci. Appl.* **2**(12), e116 (2013).
31. NanoGuide (<https://support.nanoscribe.com/hc/en-gb/articles/360009156293#T:IPDipRIndex>), "IP-Dip Tables: Refractive index of IP-Dip (liquid phase)," (2022).
32. B. Šantic, "Measurement of the refractive index and thickness of a transparent film from the shift of the interference pattern due to the sample rotation," *Thin Solid Films* **518**(14), 3619–3624 (2010).
33. L. Sewald, C. Claaßen, T. Götz, M. H. Claaßen, V. Truffault, G. E. M. Tovar, A. Southan, and K. Borchers, "Beyond the modification degree: impact of raw material on physicochemical properties of gelatin type A and type B methacryloids," *Macromol. Biosci.* **18**(12), 1800168 (2018).
34. B.-B. Xu, H. Xia, L.-G. Niu, Y.-L. Zhang, K. Sun, Q.-D. Chen, Y. Xu, Z.-Q. Lv, Z.-H. Li, H. Misawa, and H.-B. Sun, "Flexible nanowiring of metal on nonplanar substrates by femtosecond-laser-induced electroless plating," *Small* **6**(16), 1762–1766 (2010).